


Article

# Magnetic and Magneto-Caloric Properties of the Amorphous $\text{Fe}_{92-x}\text{Zr}_8\text{B}_x$ Ribbons

Xin Wang <sup>1</sup>, Qiang Wang <sup>2,3</sup>, Ben Zhen Tang <sup>2,3</sup>, Ding Ding <sup>2,3,\*</sup> , Li Cui <sup>1</sup> and Lei Xia <sup>2,3</sup>

<sup>1</sup> College of Engineering, Shanghai Polytechnic University, Shanghai 201209, China; wangxin2020@126.com (X.W.); cuili@sspu.edu.cn (L.C.)

<sup>2</sup> Institute of Materials, Shanghai University, Shanghai 200072, China; mat\_wq@shu.edu.cn (Q.W.); amtbp@yeah.net (B.Z.T.); xialei@shu.edu.cn (L.X.)

<sup>3</sup> Center for Advanced Microanalysis, Shanghai University, Shanghai 200444, China

\* Correspondence: d.ding@shu.edu.cn

Received: 28 October 2020; Accepted: 22 November 2020; Published: 25 November 2020



**Abstract:** Magnetic and magnetocaloric properties of the amorphous  $\text{Fe}_{92-x}\text{Zr}_8\text{B}_x$  ribbons were studied in this work. Fully amorphous  $\text{Fe}_{89}\text{Zr}_8\text{B}_3$ ,  $\text{Fe}_{88}\text{Zr}_8\text{B}_4$ , and  $\text{Fe}_{87}\text{Zr}_8\text{B}_5$  ribbons were fabricated. The Curie temperature ( $T_c$ ), saturation magnetization ( $M_s$ ), and the maximum entropy change with the variation of a magnetic field ( $-\Delta S_m^{\text{peak}}$ ) of the glassy ribbons were significantly improved by the boron addition. The mechanism for the enhanced  $T_c$  and  $-\Delta S_m^{\text{peak}}$  by boron addition was studied.

**Keywords:** metallic glasses; magnetocaloric effect; Curie temperature; the adiabatic temperature rise

## 1. Introduction

With the rising concerns on environmental pollution and the higher and higher cost of energy, it is an urgent need recently to develop energy-saving and environmental-friendly materials, such as new energy storage materials, magnetocaloric materials, giant impedance materials, thermoelectric materials, and magneto-strictive materials [1–5]. Magnetocaloric materials are the materials that exhibit an adiabatic temperature change when they experience a magnetization or demagnetization process, which is called the magnetocaloric effect (MCE). Magnetic refrigerators using the magnetocaloric alloys or compounds as working materials are believed to be more compact (because of solid refrigerant) and efficient (due to their lower energy consumption) than the traditional vapor compression/expansion refrigerator. Furthermore, the magnetic refrigerators are considered to be safer to the environment because they do not emit ozone-depleting gases [6,7]. Therefore, the magnetocaloric materials have recently attracted more and more attention, and as a result, a great number of magnetocaloric alloys or compounds have been developed in the past several decades [8–10].

The amorphous alloys, which exhibit higher corrosion resistance and better mechanical properties than the crystalline alloys, are considered to be suitable candidates for magnetic refrigerants because they exhibit rather broad magnetic entropy change ( $-\Delta S_m$ ) peak [11,12]. The broadened  $-\Delta S_m$  peak and the resulted high value of refrigeration capacity ( $RC$ ) lead to a rather wide working temperature range and a large amount of cooling, which is an important indicator that helps to obtain the maximum cooling capacity in the Ericsson cycle [13]. The amorphous alloys can be fabricated within a large compositional range, indicating that the Curie temperature ( $T_c$ ) and properties, depending on the alloy compositions, can be easily tuned [14].

Among the amorphous alloys that have been studied so far, Gd-based amorphous alloys and some high-entropy alloys show good reversible magnetocaloric effects [15–17]. Usually, the large maximum  $-\Delta S_m$  ( $-\Delta S_m^{\text{peak}}$ ) value of these amorphous alloys only obtained at low temperatures and their high cost limit their industrial applications. Although some amorphous alloys with reduced Gd

content can achieve application conditions in the room temperature range, they still have shortcomings in terms of cost, magnetocaloric effect, and forming ability [18,19]. In contrast, the low-cost transition metal (TM)-based amorphous alloys represented by the Fe-based amorphous alloy gained more and more attention.

In previous studies,  $\text{Fe}_{100-x}\text{B}_x$  ( $x = 12\text{--}28$ ) amorphous alloy exhibits good soft magnetic properties [20,21]. However, almost all the compositions of the Curie temperatures,  $T_c$ , are above room temperature. By adding Nb, Y, Nd, or Mn elements to amorphous system, the Curie temperature is greatly reduced, but it fails to increase the magnetic entropy change value of the alloy or even deteriorate [22]. On the other hand, FeZr binary system alloys exhibit excellent soft magnetic properties near room temperature and are accompanied with a  $-\Delta S_m^{\text{peak}}$  close to about half of the Gd [23,24]. As a result, substitution of Fe by transition metals Nb, Mn, Y, or metalloid elements B can significantly change the magnetic properties [25–27]. In particular, the addition of B can even make the alloy appear ferromagnetic near room temperature. For the purpose of meeting the requirements of magnetic refrigerants in a domestic refrigerator, recently, many multicomponent Fe-based amorphous alloys with excellent magnetocaloric properties have been synthesized based on the ternary Fe-Zr-B glass-forming alloys [27–30]. The lower Zr content Fe-B-Zr amorphous alloys usually have a lower MCE with the  $-\Delta S_m^{\text{peak}}$  about  $1.04 \text{ J K}^{-1} \text{ kg}^{-1}$  for a field change of 0–15 kOe in the  $\text{Fe}_{94-x}\text{Zr}_6\text{B}_x$  ( $x = 5, 6, 8, \text{ and } 10$ ) amorphous alloys. When the Zr content is increased, the  $\Delta S_m$  of the alloy becomes significantly improved: for instance, the magnetic properties, phase transitions, and MCE were systematically studied in amorphous  $\text{Fe}_{89-x}\text{B}_x\text{Zr}_{11}$  ( $x = 0\text{--}10$ ) alloys and the  $T_c$  got enhanced with B addition and the  $-\Delta S_m$  value to be about  $1.73 \text{ J K}^{-1} \text{ kg}^{-1}$  for the  $\text{Fe}_{79}\text{Zr}_{11}\text{B}_{10}$  sample. Meanwhile, the addition of a series of 3D elements, such as Cu, Cr, Mn, Co, Ni..., also obtained a series of FeZrB-based amorphous alloys with a good  $\Delta S_m$  value near room temperature [31–36]. Recently, related studies have shown that FeZrB(Cu,Co...) amorphous alloys also have dispersed nanocrystalline particles on the amorphous matrix [37,38]. Appropriate selection and control methods of heat treatment can make nanocrystalline particles aggregate and grow, further, by selectively removing the surface nanocrystalline particles, the amorphous materials with nanoporosity on the surface can be obtained. However, after the selective dealloying treatment of nanocrystalline amorphous alloys, it is found that the magnetization of the alloys is improved. This is mainly related to the increase in the concentration of ferromagnetic atoms in the system, which also provides a way to further improve the magnetic properties of the amorphous alloys.

Through the previous study on the  $\text{Fe}_{88}\text{Zr}_8\text{B}_4$  amorphous alloy [30,39,40], it is found that a moderate Zr content makes the alloy exhibit good magnetic properties near room temperature. However, the mechanism for their good magnetocaloric properties has not been investigated systematically. Therefore, the detailed investigation on the magnetic and magnetocaloric properties of Fe-Zr-B ternary metallic glasses may be helpful for the understanding of the tailorable magnetic and magnetocaloric properties near room temperature in the multicomponent Fe-Zr-B-based metallic glasses. In the present work, we fabricated  $\text{Fe}_{92-x}\text{Zr}_8\text{B}_x$  ( $x = 3, 4, 5$ ) amorphous samples in the shape of ribbons with an average thickness of 0.04 mm. Magnetic properties of the amorphous samples were measured and their magnetocaloric properties were obtained. The dependence of  $T_c$  as well as  $-\Delta S_m^{\text{peak}}$  on the composition of the metallic glasses were constructed for the purpose of revealing the mechanism involved.

## 2. Experiments

Alloy ingots with a nominal composition of  $\text{Fe}_{92-x}\text{Zr}_8\text{B}_x$  ( $x = 3, 4, 5$ ) were prepared by arc melting a mixture of high-purity (99.95 wt%) Fe, Zr metallic pieces and Fe-B pre-alloy for at least four times in a non-consumable electrode high vacuum arc melting furnace.  $\text{Fe}_{92-x}\text{Zr}_8\text{B}_x$  ribbons with an average thickness of  $\sim 0.04$  mm were prepared by ejecting the melts from the quartz tube to the surface of a rotating copper wheel under a pure Ar atmosphere. The surface speed of the copper wheel was optimized at 30 m/s. Structure of the ribbons was checked by X-ray diffraction (XRD) using the  $K_\alpha$  radiation of Cu on a Rigaku diffractometer (model D/max-2550) (Rigaku, Tokyo,

Japan). Thermal properties about the glass transition temperature ( $T_g$ ), crystallization temperature ( $T_x$ ) and the liquidus temperature ( $T_l$ ) of the amorphous ribbons were measured by a Netzsch DSC-404C differential scanning calorimetry (DSC) (Netzsch, Selb, Germany) under a purified argon atmosphere at a heating rate of 20 K/min. Microstructures of the amorphous ribbons were observed by a JEOL JEM-2010F (JEOL, Tokyo, Japan) high-resolution electron microscope (HREM). The specimens for HREM observations were prepared by ion-polishing under a pure argon atmosphere using the GATAN 691 precision ion-polishing system (AMETEK, Berwyn, PA, USA). Magnetic properties of the as-spun ribbons were measured by a Quantum Design Physical Properties Measurement System (Ever cool II): the temperature dependence of the magnetization (M-T) curves were obtained under a field of 0.03 T in the cooling process; hysteresis loops were measured under a field of 5 T at 10 K and 380 K, respectively; isothermal magnetization (M-H) curves were obtained at various temperatures under a field of 5 T. The heat capacity ( $C_p(T)$ ) of the  $\text{Fe}_{87}\text{Zr}_8\text{B}_5$  amorphous ribbon was also measured by PPMS near its  $T_c$  under a zero magnetic field.

### 3. Results and Discussion

X-ray diffraction patterns of the  $\text{Fe}_{92-x}\text{Zr}_8\text{B}_x$  ( $x = 3, 4, 5$ ) ribbons are presented in Figure 1. Only one typical broadened diffraction hump was observed between  $2\theta$  of  $30^\circ$  and  $35^\circ$  on each pattern; and the absence of visible crystalline peaks are present on the XRD curves of the ribbons. It indicates that the  $\text{Fe}_{92-x}\text{Zr}_8\text{B}_x$  ribbons are fully amorphous structures.

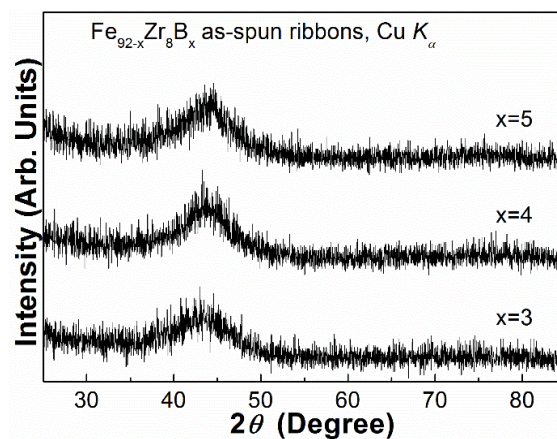
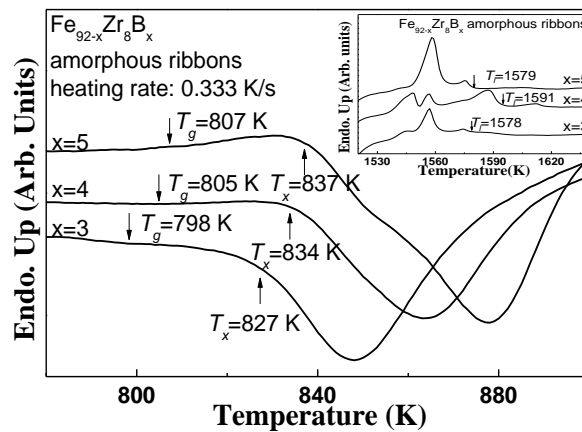


Figure 1. XRD patterns of the  $\text{Fe}_{92-x}\text{Zr}_8\text{B}_x$  ( $x = 3, 4, 5$ ) as-spun ribbons.

The amorphous feature of the  $\text{Fe}_{92-x}\text{Zr}_8\text{B}_x$  ribbons prepared under the linear velocity of 30 m/s can be further confirmed from their differential scanning calorimetry (DSC) trace (Figure 2). The obvious endothermic glass transition behaviors before the crystallization and the visible crystallization exothermic peak (see the small figure in Figure 2) also verify the amorphous characteristics of the ribbon. As seen from the DSC trace, the onset temperatures of glass transition ( $T_g$ ) of  $\text{Fe}_{92-x}\text{Zr}_8\text{B}_x$  ( $x = 3, 4, 5$ ) are about 798 K, 805 K, 807 K; and crystallization ( $T_x$ ) is about 827 K, 834 K and 837 K, respectively.

In order to verify the above assumption more intuitively, high-resolution electron microscope (HREM) micrographs of the  $\text{Fe}_{88}\text{Zr}_8\text{B}_4$  sample were performed and depicted in Figure 3. The HREM image reveals the fully amorphous characteristics with only short-range order in the disordered matrix. Similar features in XRD patterns and the DSC curves of these samples indicates the approximate structural features in all other samples studied.



**Figure 2.** Differential scanning calorimetry (DSC) traces of the  $\text{Fe}_{92-x}\text{Zr}_8\text{B}_x$  ( $x = 3, 4, 5$ ) alloys with the heating curves obtained at 20 K/min; the inset is the melt DSC trace.

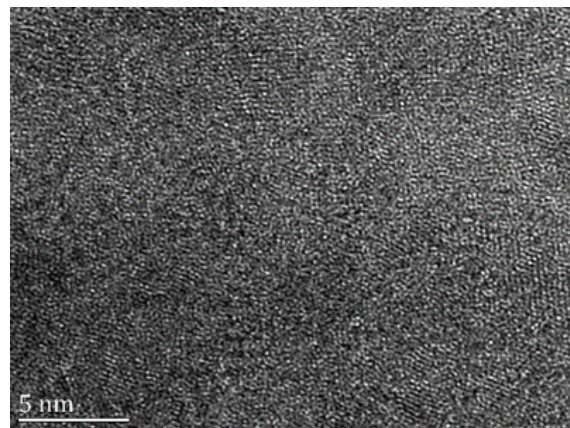


**Figure 3.** High-resolution electron microscope (HREM) micrograph of  $\text{Fe}_{88}\text{Zr}_8\text{B}_4$  sample.

Coercivity and saturation magnetization ( $M_s$ ) of the  $\text{Fe}_{92-x}\text{Zr}_8\text{B}_x$  ( $x = 3, 4, 5$ ) glassy ribbons were obtained from the hysteresis loops measured at 10 K under 5 T. As shown in Figure 4a, the nearly zero coercivity of all the  $\text{Fe}_{92-x}\text{Zr}_8\text{B}_x$  ( $x = 3, 4, 5$ ) glassy samples indicates that the metallic glasses are soft magnetic properties at 10 K.  $M_s$  of the  $\text{Fe}_{92-x}\text{Zr}_8\text{B}_x$  ( $x = 3, 4, 5$ ) glassy ribbons obtained from their hysteresis loops are about  $107.5 \text{ Am}^2/\text{kg}$  for  $x = 3$ ,  $109.2 \text{ Am}^2/\text{kg}$  for  $x = 4$ , and  $110.7 \text{ Am}^2/\text{kg}$  for  $x = 5$ , respectively. The dependence of  $M_s$  on the boron content of the three glassy samples, as plotted in the inset of Figure 4a, shows a roughly linear relationship between  $M_s$  and  $x$ . The increasing  $M_s$  with  $x$  in the  $\text{Fe}_{92-x}\text{Zr}_8\text{B}_x$  metallic glasses is most likely related to the improved Fe-B interactions with increasing B content [27,39]. The enhanced  $M_s$  implies the improvement of MCE by boron addition in the  $\text{Fe}_{92-x}\text{Zr}_8\text{B}_x$  amorphous alloys because  $M_s$  or  $-\Delta S_m$  depends on the ordering of magnetic moments in metallic glasses upon magnetization.

In addition, unlike the rare earth (RE)-transition metal (TM)-based (RE-TM-based) metallic glasses, the enhanced interaction by boron addition may result in the improvement of  $T_c$  in  $\text{Fe}_{92-x}\text{Zr}_8\text{B}_x$  glassy alloys because  $T_c$  of the Fe-based metallic glass samples primarily depend on the  $3d$ - $3d$  direct interaction [27,29,34–37]. Figure 4b shows the variation of magnetization on the temperature ( $M$ - $T$  curves) of the  $\text{Fe}_{92-x}\text{Zr}_8\text{B}_x$  glassy samples measured under 0.03 T.  $T_c$  derived from the  $M$ - $T$  curves is about 271 K for  $\text{Fe}_{89}\text{Zr}_8\text{B}_3$ , 291 K for  $\text{Fe}_{88}\text{Zr}_8\text{B}_4$ , and 306 K for  $\text{Fe}_{87}\text{Zr}_8\text{B}_5$  amorphous ribbons. The Curie temperatures of the glassy samples were located in the working temperature range of a domestic refrigerator, which indicates that the  $\text{Fe}_{92-x}\text{Zr}_8\text{B}_x$  glasses ribbons may be the good working medium of magnetic refrigeration when the  $-\Delta S_m^{\text{peak}}$  of these alloys are high enough.



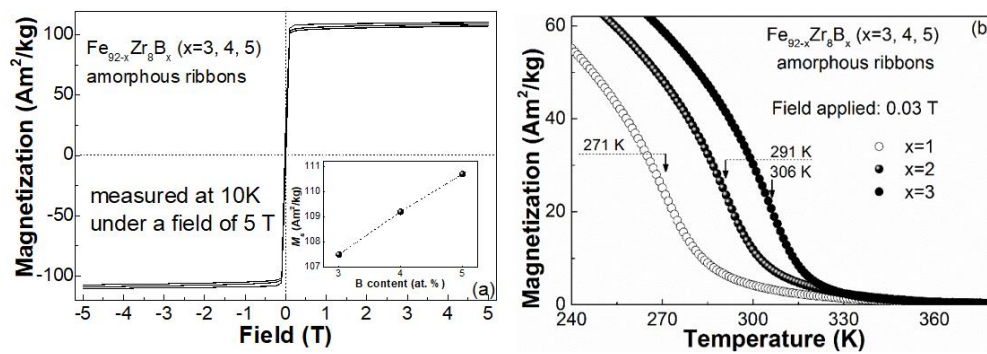


**Figure 4.** (a) Hysteresis loops of the  $\text{Fe}_{92-x}\text{Zr}_8\text{B}_x$  ( $x = 3, 4, 5$ ) amorphous ribbons measured at 10 K under a field of 5 T; the inset is the relationship between the  $M_s$  and  $x$ . (b) The  $M$ - $T$  curves of the  $\text{Fe}_{92-x}\text{Zr}_8\text{B}_x$  ( $x = 3, 4, 5$ ) amorphous alloys measured under a field of 0.03 T.

By measuring the isothermal magnetization ( $M$ - $H$ ) curves of the  $\text{Fe}_{92-x}\text{Zr}_8\text{B}_x$  glassy ribbons at various temperatures, we can calculate the  $-\Delta S_m$  of these amorphous alloys. Figure 5 shows the  $-\Delta S_m$  plots at different temperatures under the magnetic fields of 1 T, 1.5 T, 2 T, 2.5 T, 3 T, 3.5 T, 4 T, 4.5 T, and 5 T. According to the trend, with a flat and continuously changing value, shown in the  $-\Delta S_m$ - $T$  curves, it can be seen that the  $\text{Fe}_{92-x}\text{Zr}_8\text{B}_x$  ( $x = 3, 4, 5$ ) metallic glasses exhibit the secondary magnetic phase transition features of a soft magnetic alloy.  $-\Delta S_m^{\text{peak}}$  values of the glassy ribbons under 1 T, 2 T, 3 T, 4 T, and 5 T are listed in Table 1. The  $-\Delta S_m \propto H^n$  relationship for the three samples were constructed and the  $n$  values at different temperatures were obtained. Figure 6a illustrates the  $\ln(-\Delta S_m)$  vs.  $\ln(H)$  plots near the Curie temperature of the three glassy samples and their linearly fitted lines.  $n$  is about 0.771 for  $\text{Fe}_{89}\text{Zr}_8\text{B}_3$  at 270 K, 0.769 for  $\text{Fe}_{88}\text{Zr}_8\text{B}_4$  at 290 K, and 0.766 for  $\text{Fe}_{87}\text{Zr}_8\text{B}_5$  at 305 K. The values of  $n$  near  $T_c$  are approximately consistent in the alloys, and the alloys with fully amorphous structures exhibit 2nd magnetic phase transition [17,41,42]. The  $n$ - $T$  curves for the  $\text{Fe}_{92-x}\text{Zr}_8\text{B}_x$  glassy samples, seen in the inset of Figure 6a, display typical magnetocaloric behaviors of soft magnetic metallic glasses:  $n$  is nearly 1 at low temperature when the sample is ferromagnetic, then gradually reduces to a minimum value near  $T_c$ , and finally increases dramatically to a value up to 2 at the paramagnetic state [18,43].

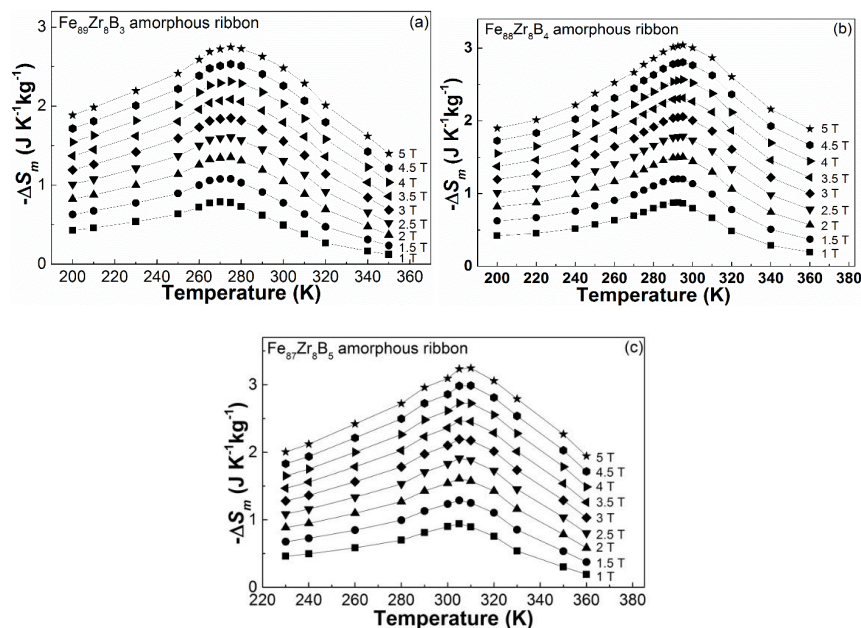


**Figure 5.**  $-\Delta S_m$ - $T$  curves of the  $\text{Fe}_{92-x}\text{Zr}_8\text{B}_x$  ( $x = 3, 4, 5$ ) amorphous ribbons under various magnetic fields: (a)  $x = 3$ , (b)  $x = 4$ , and (c)  $x = 5$ .

**Table 1.** Curie temperature,  $T_c$ , and  $-\Delta S_m^{peak}$  of the several Fe-Zr-B-based amorphous samples.

Composition	$-\Delta S_m^{peak} * (\text{J kg}^{-1} \text{K}^{-1})$					$T_c$ (K)	Ref.
	1 T	1.5 T	2 T	3 T	5 T		
Fe <sub>89</sub> Zr <sub>8</sub> B <sub>3</sub>	0.79	1.08	1.35	1.85	2.75	271	Present work
Fe <sub>88</sub> Zr <sub>8</sub> B <sub>4</sub>	0.88	1.20	1.50	2.06	3.04	291	
Fe <sub>87</sub> Zr <sub>8</sub> B <sub>5</sub>	0.94	1.29	1.61	2.19	3.25	306	
Fe <sub>88</sub> Zr <sub>9</sub> B <sub>3</sub>	0.94	1.28	1.59	2.16	3.17	286	[29]
Fe <sub>87</sub> Zr <sub>9</sub> B <sub>4</sub>	0.99	1.35	1.67	2.26	3.29	304	
Fe <sub>86</sub> Zr <sub>9</sub> B <sub>5</sub>	1.02	1.39	1.72	2.3	3.34	327	
Fe <sub>88</sub> Zr <sub>8</sub> B <sub>4</sub>	0.87	1.2	1.5	2.06	3.04	292	[34]
Fe <sub>87</sub> Co <sub>1</sub> Zr <sub>8</sub> B <sub>4</sub>	0.93	1.29	1.61	2.2	3.24	317	
Fe <sub>86</sub> Co <sub>2</sub> Zr <sub>8</sub> B <sub>4</sub>	0.98	1.35	1.69	2.31	3.38	340	
Fe <sub>87</sub> Zr <sub>8</sub> B <sub>4</sub> Sm <sub>1</sub>	0.98	1.33	1.65	2.24	3.27	308	[35]
Fe <sub>86</sub> Zr <sub>8</sub> B <sub>4</sub> Sm <sub>2</sub>	1.04	1.41	1.73	2.32	3.35	325	
Fe <sub>85</sub> Zr <sub>8</sub> B <sub>4</sub> Sm <sub>3</sub>	1.09	1.47	1.81	2.44	3.55	333	
Fe <sub>87</sub> Zr <sub>7</sub> B <sub>4</sub> Co <sub>2</sub>	1.01	1.38	1.72	2.34	3.42	333	[36]

\* The maximum magnetic entropy change ( $-\Delta S_m$ ) value in the  $-\Delta S_m$ - $T$  curves.

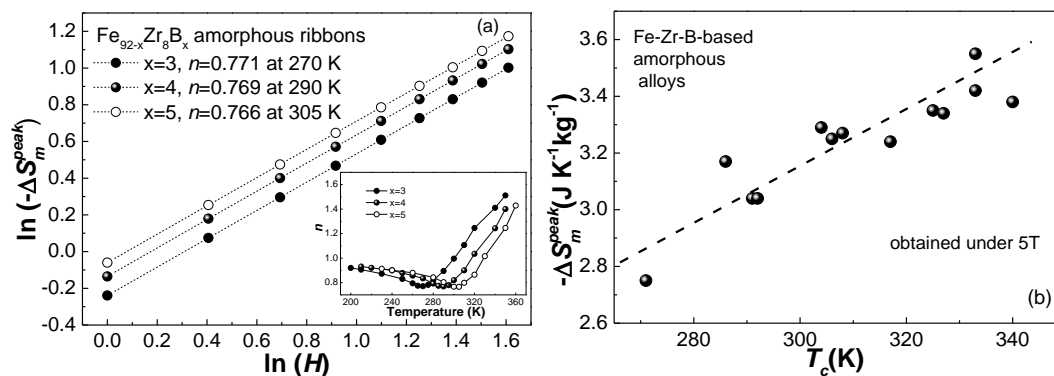


**Figure 6.** (a) The  $-\Delta S_m^{peak} \propto H^n$  relationship of the Fe<sub>91-x</sub>Zr<sub>9</sub>B<sub>x</sub> ( $x = 3, 4, 5$ ) amorphous alloys at  $T_c$ , the inset is the  $n$ - $T$  curves of the three amorphous alloys; (b) the  $-\Delta S_m^{peak}$  (under 5 T) vs.  $T_c$  plots and the linear fitting (dash line) these plots in several Fe-Zr-B-based amorphous samples (listed in Table 1).

$-\Delta S_m^{peak}$  of Fe<sub>92-x</sub>Zr<sub>8</sub>B<sub>x</sub> amorphous alloys, as predicted above, increases with boron addition:  $-\Delta S_m^{peak}$  under 5 T at  $x = 5$  is about 6.9% higher than the  $-\Delta S_m^{peak}$  value at  $x = 4$  and about 18.2% higher than the  $-\Delta S_m^{peak}$  value at  $x = 3$ . The increasing  $-\Delta S_m^{peak}$  as well as  $M_s$  with boron addition is most likely due to the exciting of free electrons in Fe atoms to a high spin state and thus strengthening the overall magnetic moments by adding of nonmagnetic B element. Therefore, the dependence of  $-\Delta S_m^{peak}$  on  $T_c$  of the Fe<sub>92-x</sub>Zr<sub>8</sub>B<sub>x</sub> metallic glasses is contrary to the  $-\Delta S_m^{peak}$ - $T_c$  relationship proposed by Belo et al. [44] in the RE-based glassy samples. The  $-\Delta S_m^{peak}$  (under 5 T) vs.  $T_c$  plots in several Fe-Zr-B-based amorphous samples (listed in Table 1), and their linear fitting (dash line) is illustrated in Figure 4b.  $-\Delta S_m^{peak}$  for these Fe-Zr-B-based glassy ribbons increases monotonically with the Curie temperature, which is possibly because the magnetic interactions in the Fe-Zr-B-based glass is not so complicated as the situation in the RE-based amorphous samples.

It is worthy to note that the Fe<sub>87</sub>Zr<sub>8</sub>B<sub>5</sub> amorphous alloy exhibits a rather high  $-\Delta S_m^{peak}$  at the temperature near 305 K. For instance, the  $-\Delta S_m^{peak}$  under 5 T of the Fe<sub>87</sub>Zr<sub>8</sub>B<sub>5</sub> glassy sample reaches to 3.25 J K<sup>-1</sup> kg<sup>-1</sup> at 305 K, which is comparable to that of the Fe<sub>87</sub>Zr<sub>8</sub>B<sub>4</sub>Sm<sub>1</sub> amorphous ribbon

( $3.27 \text{ J K}^{-1} \text{ kg}^{-1}$  at 308 K) and the  $\text{Fe}_{87}\text{Zr}_9\text{B}_4$  amorphous ribbon ( $3.29 \text{ J K}^{-1} \text{ kg}^{-1}$  at 304 K), but is larger than that of the  $\text{Fe}_{87}\text{Zr}_6\text{B}_6\text{Cu}_1$  ( $3 \text{ J K}^{-1} \text{ kg}^{-1}$  at 300 K) metallic glass [29,30,35]. In order to reveal the refrigeration efficiency of the  $\text{Fe}_{87}\text{Zr}_8\text{B}_5$  amorphous alloy, we calculate the temperature rise under an adiabatic condition ( $\Delta T_{ad}$ ) of the sample according to

$$\Delta T_{ad}(T, 0 \rightarrow H) = -\frac{T}{C_p(T)} \Delta S_m(T, 0 \rightarrow H) \quad (1)$$

The  $\Delta T_{ad}$ - $T$  curve of the  $\text{Fe}_{87}\text{Zr}_8\text{B}_5$  glassy ribbon is shown in Figure 7, the inset is the  $C_p(T)$  curve. The maximum  $\Delta T_{ad}$  for the  $\text{Fe}_{87}\text{Zr}_8\text{B}_5$  metallic ribbon is about 0.76 K under 1.5 T, and 1.98 K under 5 T, respectively.

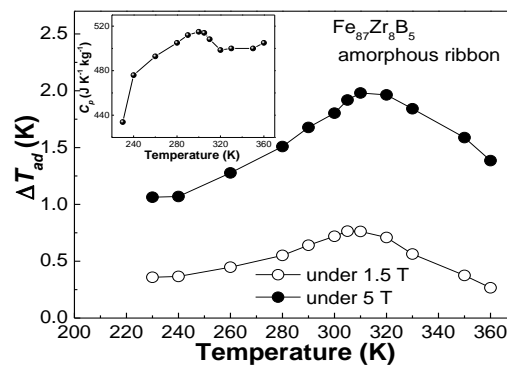


**Figure 7.**  $\Delta T_{ad}$ - $T$  curve of the  $\text{Fe}_{87}\text{Zr}_8\text{B}_5$  amorphous alloy under the fields of 1.5 T and 5 T, the inset is the  $C_p(T)$  curve of the amorphous alloy.

#### 4. Conclusions

In summary, the  $\text{Fe}_{92-x}\text{Zr}_8\text{B}_x$  ( $x = 3, 4, 5$ ) glassy ribbons were successfully prepared. The magnetic and magnetocaloric behaviors of these glassy samples were studied.  $T_c$  of the  $\text{Fe}_{92-x}\text{Zr}_8\text{B}_x$  glassy samples is about 271 K at  $x = 3$ , about 291 K at  $x = 4$ , and about 306 K at  $x = 5$ . It was found that  $T_c$ ,  $-\Delta S_m^{peak}$ , and  $M_s$  of the  $\text{Fe}_{92-x}\text{Zr}_8\text{B}_x$  amorphous samples show an increase trend with the boron content. The simultaneously increasing  $M_s$ ,  $T_c$ , and  $-\Delta S_m^{peak}$  with boron content in the  $\text{Fe}_{92-x}\text{Zr}_8\text{B}_x$  amorphous alloys is mostly likely attributed to the enhanced interaction between the Fe-B atoms by boron addition. The high  $-\Delta S_m^{peak}$  and  $\Delta T_{ad}$  of the  $\text{Fe}_{87}\text{Zr}_8\text{B}_5$  metallic ribbon near 305 K indicate that the amorphous sample may be a good candidate for the magnetic refrigerants of a domestic magnetic refrigerator.

**Author Contributions:** X.W.: Data curation, Writing—original draft. Q.W.: Data curation, Writing—original draft. B.Z.T. and L.C.: Data curation, Methodology, Writing—original draft. D.D. and L.X.: Conceptualization, Methodology, Writing—review & editing. All authors have read and agreed to the published version of the manuscript.

**Funding:** The National Nature Science Foundation of China: 51271103; the National Nature Science Foundation of China: 51701003; the National Nature Science Foundation of China: 51671119; the National Nature Science Foundation of China: 51675323; the Non-ferrous metal materials preparation and processing state key laboratory open project: 19AZ02; Shanghai Natural Science Foundation Project: 20ZR1421000; Materials Science and Engineering Discipline of Shanghai Polytechnic University: XXKZD1601.

**Acknowledgments:** The work described in this paper was supported by the National Nature Science Foundation of China (Grant Nos. 51271103, 51701003, 51671119 and 51675323), the non-ferrous metal materials preparation, and processing state key laboratory open project (Grant No. 19AZ02), Shanghai Natural Science Foundation Project (No. 20ZR1421000), and Materials Science and Engineering Discipline of Shanghai Polytechnic University (XXKZD1601).

**Conflicts of Interest:** The authors declare no conflict of interest.

## References

1. Shen, X.; Liu, H.; Cheng, X.B.; Yan, C.; Huang, J.Q. Beyond lithium ion batteries: Higher energy density battery systems based on lithium metal anodes. *Energy Storage Mater.* **2018**, *12*, 161–175. [[CrossRef](#)]
2. Gschneider, K.A.; Pecharsky, V.K. Magnetocaloric Materials. *Annu. Rev. Mater. Sci.* **2000**, *30*, 387–429. [[CrossRef](#)]
3. Phan, M.H.; Peng, H.X. Giant magnetoimpedance materials: Fundamentals and applications. *Prog. Mater. Sci.* **2008**, *53*, 323–420. [[CrossRef](#)]
4. Yang, L.; Chen, Z.G.; Dargusch, M.S.; Zou, J. High Performance Thermoelectric Materials: Progress and Their Applications. *Adv. Energy Mater.* **2018**, *8*, 1701797. [[CrossRef](#)]
5. Tang, B.Z.; Guo, D.Q.; Xia, L.; Ding, D.; Chan, K.C. Magnetoelastic and magnetocaloric properties of Tb<sub>62.5</sub>Co<sub>37.5</sub> amorphous alloy. *J. Alloys Compd.* **2017**, *728*, 747–751. [[CrossRef](#)]
6. Tishin, A.M.; Spichkin, Y.I. The magnetocaloric effect and its applications. *Inst. Phys. Bristol.* **2003**. [[CrossRef](#)]
7. de Oliveira, N.A.; von Ranke, P.J. Theoretical aspects of the magnetocaloric effect. *Phys. Rep.* **2010**, *489*, 89–160. [[CrossRef](#)]
8. Gschneider, K.A.; Pecharsky, V.K.; Tsokol, A.O. Recent developments in magnetocaloric materials. *Rep. Prog. Phys.* **2005**, *68*, 1479–1539. [[CrossRef](#)]
9. Franco, V.; Blázquez, J.S.; Ipus, J.J.; Law, J.Y.; Moreno-Ramírez, L.M.; Conde, A. Magnetocaloric effect: From materials research to refrigeration devices. *Prog. Mater. Sci.* **2018**, *93*, 112–232. [[CrossRef](#)]
10. Chaudhary, V.; Chen, X.; Ramanujan, R.V. Iron and manganese based magnetocaloric materials for near room temperature thermal management. *Prog. Mater. Sci.* **2019**, *100*, 64–98. [[CrossRef](#)]
11. Franco, V.; Conde, A. Magnetic refrigerants with continuous phase transitions: Amorphous and nanostructured materials. *Scr. Mater.* **2012**, *69*, 594–599. [[CrossRef](#)]
12. Brück, E. Developments in magnetocaloric refrigeration. *J. Phys. D Appl. Phys.* **2005**, *38*, R381–R391. [[CrossRef](#)]
13. Hashimoto, T.; Kuzuhara, T.; Matsumoto, K.; Sahashi, M.; Inomata, K.; Tomokiyo, A.; Yayama, H. New application of complex magnetic materials to the magnetic refrigerant in an Ericsson magnetic refrigerator. *J. Appl. Phys.* **1987**, *62*, 3873–3878. [[CrossRef](#)]
14. Luo, Q.; Wang, W.H. Rare earth based bulk metallic glasses. *J. Non-Cryst. Solids* **2009**, *355*, 759–775. [[CrossRef](#)]
15. Xia, L.; Tang, M.B.; Chan, K.C.; Dong, Y.D. Large magnetic entropy change and adiabatic temperature rise of a Gd<sub>55</sub>Al<sub>20</sub>Co<sub>20</sub>Ni<sub>5</sub> bulk metallic glass. *J. Appl. Phys.* **2014**, *115*, 223904. [[CrossRef](#)]
16. Tang, B.Z.; Huang, L.W.; Song, M.N.; Ding, D.; Wang, X.; Xia, L. Compositional dependence of magnetic and magnetocaloric properties of the Gd-Ni binary amorphous alloys. *J. Non-Cryst. Solids* **2019**, *522*, 119589. [[CrossRef](#)]
17. Huo, J.T.; Huo, L.H.; Li, J.W.; Men, H.; Wang, X.M.; Inoue, A.; Chang, C.T.; Wang, J.Q.; Li, R.W. High-entropy bulk metallic glasses as promising magnetic refrigerants. *J. Appl. Phys.* **2015**, *117*, 073902. [[CrossRef](#)]
18. Tang, B.Z.; Xie, H.X.; Li, D.M.; Xia, L.; Yu, P. Microstructure and its effect on magnetic and magnetocaloric properties of the Co<sub>50</sub>Gd<sub>50-x</sub>Fe<sub>x</sub> glassy ribbons. *J. Non-Cryst. Solids* **2020**, *533*, 119935. [[CrossRef](#)]
19. Wang, X.; Tang, B.Z.; Wang, Q.; Yu, P.; Ding, D.; Xia, L. Co<sub>50</sub>Gd<sub>48-x</sub>Fe<sub>2</sub>Ni<sub>x</sub> amorphous alloys with high adiabatic temperature rise near the hot end of a domestic magnetic refrigerator. *J. Non-Cryst. Solids* **2020**, *544*, 120146. [[CrossRef](#)]
20. Hasegawa, R.; Ray, R. Iron-boron metallic glasses. *J. Appl. Phys.* **1978**, *49*, 4174–4179. [[CrossRef](#)]
21. O’Handley, R.C. Physics of ferromagnetic amorphous alloys. *J. Appl. Phys.* **1987**, *62*, R15. [[CrossRef](#)]
22. Waske, A.; Schwarz, B.; Mattern, N.; Eckert, J. Magnetocaloric (Fe-B)-based amorphous alloys. *J. Magn. Magn. Mater.* **2013**, *329*, 101–104. [[CrossRef](#)]
23. Maeda, H.; Sato, M.; Uehara, M. Fe-Zr Amorphous Alloys for Magnetic Refrigerants near Room Temperature. *J. Jpn. Inst. Met.* **1983**, *47*, 688–691. [[CrossRef](#)]
24. Wang, Y.Y.; Hou, K.; Bi, X. Hydrogenated Fe<sub>90</sub>M<sub>10</sub> (M: Zr and Sc) amorphous alloys with enhanced room-temperature magnetocaloric effect. *J. Alloys Compd.* **2016**, *689*, 564–569. [[CrossRef](#)]
25. Min, S.G.; Kim, K.S.; Yu, S.C.; Suh, H.S.; Lee, S.W. Analysis of magnetization and magnetocaloric effect in amorphous FeZrMn ribbons. *J. Appl. Phys.* **2005**, *97*, 10M310. [[CrossRef](#)]
26. Kim, K.S.; Min, S.G.; Yu, S.C.; Oh, S.K.; Kim, Y.C.; Kim, K.Y. The large magnetocaloric effect in amorphous Fe<sub>91-x</sub>Y<sub>x</sub>Zr<sub>9</sub> (x=0, 5, 10) alloys. *J. Magn. Magn. Mater.* **2006**, *304*, E642–E644. [[CrossRef](#)]



27. Mishra, D.; Gurram, M.; Reddy, A.; Perumal, A.; Saravanan, P.; Srinivasan, A. Enhanced soft magnetic properties and magnetocaloric effect in B substituted amorphous Fe-Zr alloy ribbons. *Mater. Sci. Eng. B* **2010**, *175*, 253–260. [[CrossRef](#)]
28. Guo, D.Q.; Chan, K.C.; Xia, L.; Yu, P. Magneto-caloric effect of  $\text{Fe}_x\text{Zr}_y\text{B}_{100-x-y}$  metallic ribbons for room temperature magnetic refrigeration. *J. Magn. Magn. Mater.* **2017**, *423*, 379–385. [[CrossRef](#)]
29. Yu, P.; Zhang, J.Z.; Xia, L. Effect of boron on the magneto-caloric effect in  $\text{Fe}_{91-x}\text{Zr}_9\text{B}_x$  ( $x=3, 4, 5$ ) amorphous alloys. *J. Mater. Sci.* **2017**, *52*, 13948–13955. [[CrossRef](#)]
30. Alvarez-Alonso, P.; Sánchez Llamazares, J.L.; Sánchez-Valdés, C.F.; Fdez-Gubieda, M.L.; Gorria, P.; Blanco, J.A. High-magnetic field characterization of magnetocaloric effect in FeZrB(Cu) amorphous ribbons. *J. Appl. Phys.* **2015**, *117*, 17A710. [[CrossRef](#)]
31. Li, X.Z.; Pan, Y. Magnetocaloric effect in Fe-Zr-B-M ( $M = \text{Ni, Co, Al, and Ti}$ ) amorphous alloys. *J. Appl. Phys.* **2014**, *116*, 093910. [[CrossRef](#)]
32. Kiss, L.F.; Kemeny, T.; Franco, V.; Conde, A. Enhancement of magnetocaloric effect in B-rich FeZrBCu amorphous alloys. *J. Alloys Compd.* **2015**, *622*, 756–760. [[CrossRef](#)]
33. Fang, Y.K.; Yeh, C.C.; Hsieh, C.C.; Chang, C.W.; Chang, H.W.; Chang, W.C.; Li, X.M.; Li, W. Magnetocaloric effect in Fe-Zr-B-M ( $M = \text{Mn, Cr, and Co}$ ) amorphous systems. *J. Appl. Phys.* **2009**, *105*, 07A910. [[CrossRef](#)]
34. Gan, L.H.; Ma, L.Y.; Tang, B.Z.; Ding, D.; Xia, L. Effect of Co substitution on the glass forming ability and magnetocaloric effect of  $\text{Fe}_{88}\text{Zr}_8\text{B}_4$  amorphous alloys. *Sci. China Phys. Mech. Astro.* **2017**, *60*, 076121. [[CrossRef](#)]
35. Chen, L.S.; Zhang, J.Z.; Lin, W.; Yu, P.; Xia, L. Outstanding magnetocaloric effect of  $\text{Fe}_{88-x}\text{Zr}_8\text{B}_4\text{Sm}_x$  ( $x=0, 1, 2, 3$ ) amorphous alloys. *Sci. China-Phys. Mech. Astro.* **2018**, *61*, 056121. [[CrossRef](#)]
36. Yu, P.; Zhang, J.Z.; Xia, L.  $\text{Fe}_{87}\text{Zr}_7\text{B}_4\text{Co}_2$  amorphous alloy with excellent magneto-caloric effect near room temperature. *Intermetallics* **2018**, *95*, 85–88. [[CrossRef](#)]
37. Zhang, H.Y.; Fornell, J.; Feng, Y.P.; Golvano, I.; Baró, M.D.; Pellicer, E.; Sort, J. Inducing surface nanoporosity on Fe-based metallic glass matrix composites by selective dealloying. *Mater. Charact.* **2019**, *153*, 46–51. [[CrossRef](#)]
38. Nagase, T.; Yokoyama, A.; Umakoshi, Y. In situ TEM observation of the glass-to-liquid transition of metallic glass in Fe-Zr-B-Cu alloy. *Scr. Mater.* **2010**, *63*, 1020–1023. [[CrossRef](#)]
39. Álvarez, P.; Gorria, P.; Marcos, J.S.; Barquín, L.F.; Blanco, J.A. The role of boron on the magneto-caloric effect of FeZrB metallic glasses. *Intermetallics* **2010**, *18*, 2464–2467. [[CrossRef](#)]
40. Álvarez, P.; Marcos, J.S.; Gorria, P.; Barquín, L.F.; Blanco, J.A. Magneto-caloric effect in FeZrB amorphous alloys near room temperature. *J. Alloys Compd.* **2010**, *504*, S150–S154. [[CrossRef](#)]
41. Franco, V.; Blázquez, J.S.; Conde, A. The influence of Co addition on the magnetocaloric effect of Nanoperm-type amorphous alloys. *J. Appl. Phys.* **2006**, *100*, 064307. [[CrossRef](#)]
42. Banerjee, S.K. On a generalized approach to first and second order magnetic transitions. *Phys. Lett.* **1964**, *12*, 16–17. [[CrossRef](#)]
43. Law, J.Y.; Franco, V.; Moreno-Ramírez, L.M.; Conde, A.; Karpenkov, D.Y.; Radulov, I.; Skokov, K.P.; Gutfleisch, O. A quantitative criterion for determining the order of magnetic phase transitions using the magnetocaloric effect. *Nat. Commun.* **2018**, *9*, 2680. [[CrossRef](#)] [[PubMed](#)]
44. Bloie, J.H.; Amaral, J.S.; Pereira, A.M.; Amaral, V.S.; Araujo, J.P. On the Curie temperature dependency of the magnetocaloric effect. *Appl. Phys. Lett.* **2012**, *100*, 242407. [[CrossRef](#)]

**Publisher’s Note:** MDPI stays neutral with regard to jurisdictional claims in published maps and institutional affiliations.



© 2020 by the authors. Licensee MDPI, Basel, Switzerland. This article is an open access article distributed under the terms and conditions of the Creative Commons Attribution (CC BY) license (<http://creativecommons.org/licenses/by/4.0/>).